Predicted Effects of Polydispersity on the Dielectric Normal-Mode Relaxation of Entangled *cis*-Polyisoprene Melts

Jeffrey S. Fodor and Davide A. Hill*

Department of Chemical Engineering, University of Notre Dame, Notre Dame, Indiana 46556

Received May 25, 1993; Revised Manuscript Received June 30, 1993•

ABSTRACT: The effects of polydispersity on the dielectric normal-mode spectrum of *cis*-polyisoprene melts above entanglement were examined theoretically and experimentally. We explored combinations of two mixing rules, (1) linear and (2) "double reptation", and three relaxation functions, (1) reptation, (2) des Cloiseaux's "time-dependent diffusion" (TDD) and (3) a variant of TDD. Loss spectra of five samples were predicted on the basis of the sole knowledge of (1) molecular weight distributions as measured by size exclusion chromatography, (2) the molecular weight dependence of the dielectric relaxation time, and (3) the magnitude and peak frequency of a reference spectrum. Within the range of molecular weights explored, quantitative predictions were obtained for all five samples only for the case of linear mixing and simple reptation.

Introduction

The dynamic response of a polymer melt can be dramatically influenced by composition. Strong polydispersity effects on steady-shear viscosity,[1] compliance,[2] linear viscoelastic moduli,[3,4] and extensional properties[5] of flexible polymers have been well documented. Although to some extent important for low molecular weight melts, polydispersity is known to be especially crucial for entangled systems. The linear viscoelastic properties of monodisperse, linear, flexible polymers in the entangled state are generally well described by the Doi–Edwards (DE) theory of reptation,[6] based on the ideas of de Gennes.[7] Several extensions and modifications of the DE theory have been proposed to account for polydispersity. Doi and Edwards themselves suggested a linear mixing rule for the relaxation modulus, $G(t)$:[8]

$$G(t) = G_p\sum_{i=1}^{n}\phi_i\psi(t/\tau_i) \tag{1}$$

where G_p is the plateau modulus, ϕ_i and τ_i are the volume fraction and relaxation time of species i, respectively, and

$$\psi(t/\tau_i) = \frac{8}{\pi^2}\sum_{\substack{p=1\\ p\ \text{odd}}}^{\infty}\frac{\exp(-p^2t/\tau_i)}{p^2} \tag{2}$$

is the autocorrelation function of the end-to-end vector[6] of species i, as predicted by reptation. Equation 2 is identical to the autocorrelation function for Rouse normal-mode relaxation.[6,9,10] Henceforth, we will refer to eq 1 as the Doi–Edwards (DE) mixing rule and to eq 2 as the Doi–Edwards–Rouse (DER) relaxation function, respectively.

Equation 1 hinges on the idea that each species in a melt relaxes independently of the others. Viscoelastic studies,[11] however, show strong nonlinear effects of composition, indicating that polydispersity can affect the rate of renewal of the topological network constraining the chains. Mechanisms such as "constraint release"[6,12–14] and "tube dilation"[14,15] have been extensively explored as additional relaxation pathways in polydisperse systems, but only recently were analytical results of practical use obtained.

des Cloizeaux,[16] Tsenoglou,[17] and Marrucci[15] considered independently the implications of polydispersity on chain reptation and converged on identical predictions for the rheological mixing rule:

$$G(t) = G_p(\sum_{i=1}^{n}\phi_i[\psi(t/\tau_i)]^{1/2})^2 \tag{3}$$

This result was independent of the assumed chain relaxation function, $\psi(x)$. Henceforth we will refer to eq 3 as the Tsenoglou mixing rule, as proposed by Wassermann and Graessley.[11] Rheological evidence supporting eq 3 has been provided by Tsenoglou[17] using data by Struglinski and Graessley,[3] and Wasserman and Graessley.[11]

Wasserman and Graessley considered several combinations of mixing rules and relaxation functions to predict complex moduli of melts with known molecular weight distribution. Tsenoglou's mixing rule with des Cloizeaux's "time-dependent diffusion" (TDD) relaxation function gave quantitative agreement with experiments, but only for the case in which the molecular weight distribution was known exactly. Predictions based on size exclusion chromatography (SEC) data were less accurate, but still in fair agreement with experiments.

Granted the success of these microstructural models for rheological predictions, it is natural to enquire whether or not such results can be extended to other observables linked to reptation dynamics and influenced by melt polydispersity. Such an orthogonal view could provide further insight into the basic mechanism of reptation and perhaps suggest new ways to interpret existing information. This is the theme of the present article, where we consider the prediction of dielectric normal-mode relaxation in polydisperse melts of *cis*-polyisoprene, a flexible type A polymer.

In a type A polymer (as classified by Stockmayer[18]) the segmental dipoles project along the backbone in a head-to-tail configuration and sum vectorially to a global dipole moment proportional to the end-to-end vector of the chain.[19–21] The autocorrelation function of the end-to-end vector is then linked to the transient dielectric permittivity of the material[21–23] and can be measured dielectrically. The dielectric loss spectrum of a type A polymer shows two distinct peaks. Normal-mode relax-

* To whom correspondence should be addressed.
• Abstract published in *Advance ACS Abstracts*, September 1, 1993.

0024-9297/93/2226-5379$04.00/0

ation emerges as a low-frequency peak with a position and magnitude strongly dependent on polymer molecular weight and polydispersity. The high-frequency "segmental" peak is insensitive to such variables because it reflects motion of the components of the segmental dipoles perpendicular to the backbone, which lack long-range correlation. Polydispersity broadens and lowers the normal-mode peak but leaves the segmental peak intact.[19,20,24-27]

The dielectric normal-mode process in melts and solutions of *cis*-PI has been extensively characterized.[19,20,22-27] *cis*-PI is an ideal polymer for dielectric studies, due to its very small, yet measurable, segmental dipole moment. (The static dielectric constant of *cis*-PI is about 2.5, comparable to that of linear alkanes.) Because dipole–dipole interactions are weak, the system is electrically dilute even in the entangled melt state, and dielectric relaxation truly mirrors the reequilibration of the individual *cis*-PI chains.[25] This is an important point, since des Cloizeaux's and Tsenoglou's theories (perhaps the most successful viscoelastic theories to date) hinge heavily on the concept of binary interactions (entanglements) to explain polydispersity effects.[15-17] Accordingly, the relaxation modulus weighs the autocorrelation functions of the various species in a nonlinear fashion. Conversely, the dielectric permittivity of *cis*-PI should reflect a linear superposition of the separate contributions from the individual chains. (Note that this does not exclude the possibility of changes in relaxation time of the individual species with composition. Exploring this possibility is one of the objectives of this paper.) In other words, while dielectric relaxation tests the individual chains, stress relaxation reflects the entanglements between the chains. Therefore, careful examination of the effects of polydispersity on both dielectric and viscoelastic properties may allow us to attain a broader perspective over the mechanism of entanglement.

Adachi and co-workers[26] performed mechanical and dielectric loss measurements on *cis*-PI melts with narrow molecular weight distribution and noted strong similarities between the corresponding normal-mode spectra. The dielectric and viscoelastic relaxation times differed by a factor of 2, the former being the largest, in agreement with Zimm's theory.[10] Also, both times scaled with the second power of molecular weight below entanglement, and with a 3.7 power above. Adachi and co-workers[26] argued that, as dictated by reptation theory, the momentum and dipolar relaxation functions of a type A polymer should both be proportional to the autocorrelation function of the end-to-end vector, $\psi(t) = \langle \mathbf{r}(\theta)\cdot\mathbf{r}(t+\theta)\rangle/\langle \mathbf{r}^2\rangle$. Mechanical and dielectric normal-mode spectra should then mirror each other and yield identical relaxation-time spectra. Upon performing a comparison, Adachi et al.[26] noted appreciable structural differences between the spectra and concluded that the two processes are not entirely equivalent. The comparison was not entirely congruent, however, since, in an effort to minimize the influence of glassy modes on the mechanical relaxation-time spectra, the authors compared dielectric loss data of a sample with M_w = 140 kg/mol with shear loss data of a sample with M_w = 626 kg/mol. The polydispersity indices of both samples were identical (M_w/M_n = 1.05), but this does not guarantee the same for the shapes of the molecular weight distributions (MWDs). As discussed later on, polydispersity and the shape of the MWD can be important even down to M_w/M_n = 1.05.

In an earlier study, Imanishi et al.[24] investigated the effects of polydispersity by comparing the half-widths of dielectric loss peaks of *cis*-PI samples of different M_w/M_n. They found that extrapolation of the half-widths to M_w/M_n = 1 led to a value that agreed with the tube model for the low-frequency side of the spectrum, but on the high-frequency side the extrapolation fell about 10% higher than expected. We believe this discrepancy can be justified by unaccounted polydispersity effects and experimental error.

For one of their samples the authors reported a polydispersity of 1.05, implying an experimental resolution of better than ±2.5%. From their Figure 8 in ref 24, however, vertical and horizontal scatters of at least ±10% and ±3% are evident, respectively, which means that the discrepancy may have been well within experimental error. Additionally, linear extrapolation of the half-widths to M_w/M_n = 1 was not entirely justified within their range of polydispersities (we will clearly demonstrate this point in an upcoming paper). Therefore, reptation theory seems to work within a margin of uncertainty of about 10%.

Adachi et al.[27] also studied dielectric normal-mode relaxation in binary mixtures of *cis*-PI with widely separated molecular weights. They reported that the molecular weight dependence of the normal-mode relaxation time of large, semidilute (5% by wt) test chains depended on the molar mass of the small chains comprising the matrix. This indicates that, in bimodal systems characterized by a large, well-defined separation between molecular weights the relaxation time of the species can depend on matrix constitution. In such extreme circumstances linear mixing should then be inappropriate.

Despite the general success of the reptation model a puzzling discrepancy still remains, namely, the dependence of the viscoelastic relaxation time, τ_{ve}, on polymer molecular weight, M. While theory predicts $\tau_{ve} \sim M^3$, experiments consistently show a larger exponent, typically around 3.4.[28] This discrepancy holds for the dielectric normal-mode relaxation time, τ_{dnm}, also.[20] For *cis*-polyisoprene the dielectric and viscoelastic relaxation times scale both as the 3.70 ± 0.30 power of molecular weight.[20,22,24,29] Many explanations have been offered, but no general consensus exists as to the nature of this phenomenon. An early proposal by Doi[6] hinged on the idea of "contour length fluctuations" but left the basic reptation equation unscathed. des Cloizeaux[16] modeled the "non-Fickian" relaxation of chain ends as a time-dependent-diffusion (TDD) process and obtained an analytical expression for the end-to-end vector autocorrelation function. des Cloizeaux's function approaches the Doi–Edwards limit only at extremely high molecular weights, well above entanglement. For lower molecular weights, but still above entanglement, the theory correctly predicts a power law dependence

$$\tau = \tau_0(M/M_0)^n \qquad (4)$$

where τ_0 and M_0 are the reference relaxation time and molecular weight, respectively, and n is close to 3.4.[16] The transition of the power law exponent from 3.4 to the reptation limit of 3 is controlled by a parameter, M^*, which must be determined experimentally. Wasserman and Graessley assumed in their calculations $M^* = 12.5M_e$ (M_e = entanglement molecular weight) and, in some cases, obtained very good agreement with experiments.[11] des Cloizeaux's theory improves over basic reptation, in that it yields automatically a more realisitic function $\tau(M)$. Yet, from a pragmatic point of view the model does contain an adjustable parameter, M^*. In using the basic reptation model (eq 2) to predict viscoelastic or dielectric properties one is faced with a potential inconsistency regarding the

choice of the numerical value of n in eq 4. Conceptually, $n = 3$ would be the only congruent choice. On the other hand, experimentally $n > 3$, even in the monodisperse limit. For polydisperse systems the choice of n is very important, since both the shape and frequency position of the loss peaks are affected. For a known MWD, fixing n implies fixing at once the shape and position of the loss maxima. Varying M^* in des Cloizeaux's TDD model has practically the same consequences as varying n in the basic reptation model. Therefore, selection of either n or M^* on the basis of experiments is, after all, legitimate. In all of our calculations involving eq 4 we have chosen $n = 3.70$, consistent with experiments.[20,22,24,29]

In this article we attempt the prediction of dielectric spectra of moderately polydisperse *cis*-PI melts above entanglement from the measured molecular weight distributions. We examine a number of combinations of mixing rules and relaxation functions and compare the predictions to experimental data. We use the Doi–Edwards (linear),[8] and Tsenoglou's[17] mixing rules with the relaxation functions from Doi–Edward's reptation[6] and des Cloizeaux's[16] time-dependent diffusion.

In the next section all relevant theoretical results are briefly summarized, and details about the calculations are provided. A comparison between predictions and experiments follows. A discussion of the results concludes our paper.

Theory

The normal-mode contribution to the complex dielectric permittivity of a type A polymer, $\tilde{\epsilon} = \epsilon' - i\epsilon''$, can be obtained from the Fourier transform of the autocorrelation function of the end-to-end vector, $\psi(t)$:[22,23]

$$\tilde{\epsilon} = \epsilon_\infty + (\epsilon_0 - \epsilon_\infty)\int_0^\infty -\frac{d\psi}{dt} e^{-i\omega t}\, dt \tag{5}$$

where, ϵ_0 and ϵ_∞ are the zero- and infinite-frequency permittivities, respectively, ω is frequency, and t is time. In conformity with reptation theory[6] the autocorrelation functions of momentum and dipolar relaxation should both be proportional to $\psi(t)$. Accordingly, the complex shear modulus, $G = G' + iG''$, should also be obtainable from eq 5 by stipulating the equivalence $(\tilde{\epsilon} - \epsilon_\infty) \Rightarrow G$ and $(\epsilon_0 - \epsilon_\infty) \Rightarrow G_p$, where G_p is the plateau modulus.

Calculation of the relaxation function for a polydisperse system, $\psi(t)$, requires knowledge of a mixing rule. The following mixing rules will be considered here

$$\psi(t) = \sum_{i=1}^{n} \phi_i \psi(t/\tau_i) \qquad \text{Doi–Edwards (DE)} \tag{6}$$

$$\psi(t) = \left(\sum_{i=1}^{n} \phi_i [\psi(t/\tau_i)]^{1/2}\right)^2 \qquad \text{Tsenoglou} \tag{7}$$

The appropriate expression for the single-chain autocorrelation function $\psi(t/\tau_i)$ must also be specified. Two models for $\psi(t/\tau_i)$ will be considered here: (1) the Doi–Edwards–Rouse (DER) function in eq 2 and (2) des Cloizeaux's time-dependent-diffusion (TDD) model. The latter gives

$$\psi(t,\tau_i) = [\varphi(t,\tau_i)]^2 \tag{8}$$

where

$$\varphi(t,\tau_i) = \frac{8}{\pi^2}\sum_{\substack{p=1\\ p\ \text{odd}}}^{\infty} \frac{1}{p^2} \exp\left[-p^2\left(\frac{t}{\tau_i} + \frac{1}{H_i} g\left(H_i \frac{t}{\tau_i}\right)\right)\right] \tag{9}$$

$$g(x) = \sum_{n=1}^{\infty} \frac{1 - \exp(-n^2 x)}{n^2} \tag{10}$$

$$H_i = \frac{M_i}{M^*} \tag{11}$$

$$\tau_i = \tau^* H_i^3 \tag{12}$$

In the last two equations M^* and τ^* are a reference molecular weight and relaxation time, respectively, to be determined experimentally. In conjunction with the DER relaxation function (eq 2), eq 4 with $n = 3.70$ will be assumed here to hold also for the individual species in a polydisperse mixture.[11] Selection of parameters M_0 and τ_0 will be discussed later on.

Combination of eqs 6 or 7 with eqs 2, 4, or 8–12 enables calculation of $\psi(t)$ for a mixture of assigned molecular weight distribution. The frequency-dependent dielectric storage, ϵ', and loss, ϵ'', are then calculated from eq 5 as follows:

$$\epsilon'(\omega) - \epsilon_\infty = (\epsilon_0 - \epsilon_\infty)\left(1 - \int_0^\infty \psi(z/\omega)\sin(z)\, dz\right) \tag{13}$$

$$\epsilon''(\omega) = (\epsilon_0 - \epsilon_\infty)\int_0^\infty \psi(z/\omega)\cos(z)\, dz \tag{14}$$

where we have used the conditions $\psi(0) = 1$ and $\psi(t \to \infty) \to 0$.

Inspection of eqs 13 and 14 reveals two important features: (1) eq 14 contains one less parameter than eq 13 (ϵ_∞); (2) because $(\epsilon_0 - \epsilon_\infty)/\epsilon_\infty \ll 1$, ϵ'' is endowed with a much greater sensitivity to the details of the molecular weight distribution than ϵ'. Consequently, ϵ'' provides a more sensitive test for comparison between theory and experiments. Accordingly, only prediction of ϵ'' will be considered here.

The quantity $(\epsilon_0 - \epsilon_\infty)$ in eqs 13 and 14 is the dielectric strength, which, for type A polymers is given by[21,24]

$$(\epsilon_0 - \epsilon_\infty) = \frac{\langle r^2\rangle}{M}\frac{4\pi N_A \mu_{0\|}^2 \rho}{3kT} \tag{15}$$

where N_A is Avogadro's number, $\mu_{0\|}$ is the backbone component of the segmental dipole moment, $\langle r^2\rangle$ is the mean-square end-to-end distance of the chain and ρ, k, T, and M are density, Boltzmann constant, temperature, and molecular weight, respectively. For random-coil polymers $\langle r^2\rangle \propto M$ and the dielectric strength is predicted and observed[24] to be independent of M. In our predictions $(\epsilon_0 - \epsilon_\infty)$ will be treated as a constant. (Strictly speaking, $(\epsilon_0 - \epsilon_\infty)$ still depends weakly on M through the density, ρ; above entanglement the effect is negligible, however.)

The integral in eq 14 can be easily carried out analytically for the DE mixing rule and DER relaxation function, giving

$$\epsilon''(\omega) = (\epsilon_0 - \epsilon_\infty)\sum_{i=1}^{n} \phi_i \vartheta(\omega\tau_i) \tag{16}$$

where

$$\vartheta(\omega\tau_i) = \int_0^\infty \psi(z/\omega)\cos(z)\, dz = \frac{8}{\pi^2}\sum_{\substack{p=1\\ p\ \text{odd}}}^{\infty} \frac{\omega\tau_i}{p^4 + (\omega\tau_i)^2} \tag{17}$$

The accuracy of the calculations depends critically on the

number of terms chosen in the summation of eq 17. Although important especially at high frequencies, summation errors can be relevant even at moderate frequencies, say 10 times the peak value. For example, use of only the first term ($p = 1$) against the first two terms ($p = 1, 3$) will lead to a relative error of 50% at $\omega\tau = 10$. Therefore, approximation of the DER autocorrelation function (eq 2) to a single exponential in time space can lead to severely erroneous results in frequency space. To improve accuracy and reduce computation time, function $\vartheta(\omega\tau)$ in eq 17 was stored as a data array in terms of $\omega\tau$. Values of the function were then interpolated from the array as needed. This procedure significantly reduced computation time, and it proved to be as accurate as direct computation.

In calculations involving the Tsenoglou mixing rule the integral in eq 14 could not be carried out analytically and was thus performed numerically using a standard routine. Integration required some care to preserve the correct behavior of the autocorrelation function at small times (which controls the high-frequency region of the spectrum). Both the DER and the TDD relaxation functions (eq 2 and eqs 8–12, respectively) require the summation of a large number of terms at small times, due to the slow convergence of the series. (Errors due to an insufficient number of summation terms are also crucial in eqs 9 and 10.) In order to reduce computation times, asymptotic expansions valid for small times were derived for the summations in eqs 2, 9, and 10, as discussed in Appendix A. At high frequencies numerical integration of eq 10 becomes highly inefficient and inaccurate due to the rapid oscillation of the cosine function. We were able to derive an asymptotic expression for the integral in the high-frequency limit, as described in Appendix B. All of these approximations were tested for the case of the DER relaxation function and DE mixing rule (for which an exact analytical expression is available) and, occasionally, by "brute-force" numerical integration with a vectorized algorithm. In all cases the approximations proved to be extremely accurate. (Similar comparisons were also performed for the des Cloizeaux monodisperse case for several values of H (eqs 8–12). The computed spectra agreed with the calculations of des Cloizeaux.[16] We also repeated des Cloizeaux's calculations for bi-disperse mixtures as reported in ref 16. Again, no differences could be found.)

Experiments

Material Characterization. The samples used in this study originated from two sources. The samples denoted by Lir30 and Lir50 are of commercial origin and were obtained from Kuraray Co. Ltd., Japan. Samples PI-40 and PI-20 were synthesized anionically[30] in our laboratory. A fifth sample, M1, was also prepared by combining Lir30 with Lir50 to form an approximately 50/50 by wt mixture. The mixture was prepared by first dissolving the two polymers in toluene to about 50 wt % polymer. The system was mixed thoroughly and vacuum-dried at room temperature. The commercial samples had a reported content of 0.10 wt % BHT (2,6-di-*tert*-butyl-4-methylphenol) antioxidant, while the samples produced in our laboratory were stabilized with 0.40 wt % phenyl-β-naphthylamine.

The polymers were all characterized by size exclusion chromatography (SEC) in toluene at 30 °C, using a Waters instrument with a differential refractometer detector and Millipore columns. The elution curves were calibrated with *cis*-PI standards purchased from Polymer Laboratories Inc. Calibration was repeated several times at increasing dilutions to ensure reproducibility; 10 standards with molecular weights ranging from 1.30 to 3300 kg/mol were used. Several calibration curves were averaged together and the standards' molecular weights were then back-calculated. The standard deviation between calculated and nominal molecular weights within the entire molecular weight range was about 5%. (Standard deviations were calculated on groups of four consecutive points among 24 data points, to explore possible variations with molecular weight. No significant variations from the 5% level were found.) Chain microstructures (% cis, % trans, % vinyl) were determined by proton NMR as described in ref 31. M_w, polydispersity indices, and chain compositions for each of the samples are listed in Table I.

Table I. Characteristics of *cis*-Polyisprene Samples

			Microstructures (mol %)[a]		
sample	M_w[b]	M_w/M_n	cis-1,4	trans-1,4	vinyl-3,4
Lir30	22.1	1.39	62.5	30.1	7.4
Lir50	43.3	1.33	62.8	30.8	6.4
PI-20	19.2	1.25	68.5	25.4	6.2
PI-40	41.6	1.30	68.7	24.8	6.5

[a] Determined by proton NMR. [b] In kg/mol.

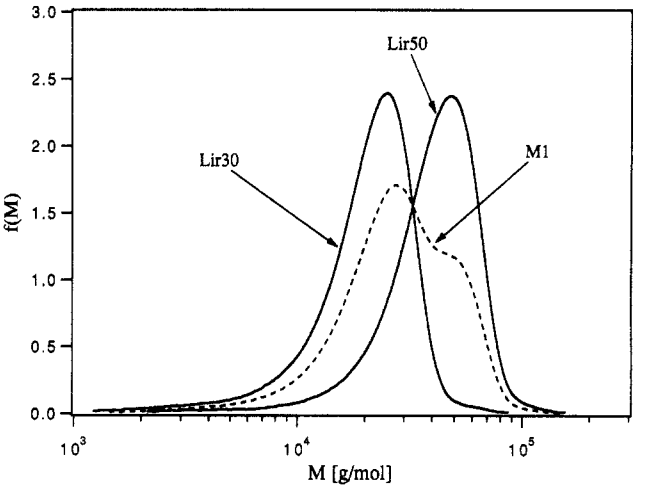

Figure 1. Differential molecular weight distributions of Lir30, Lir50, and M1, expressed as $f(M_i) = M_i\phi_i$.

Molecular weight distributions were extracted directly from the SEC data. Samples of increasing dilution were occasionally run to verify reproducibility of the distributions. The flow rate was also reduced occasionally to improve resolution. No statistically-significant changes were resolved. Volume and weight fraction are experimentally indistinguishable above entanglement,[11] so that refractometry data can be used as a direct measure of weight fraction. The volume fractions, ϕ_i, pertaining to a given range of molecular weights centered around M_i were obtained by integration of discrete slices under the MWD curve. At least 100 logarithmically-spaced slices were used for each distribution (spanning typically two decades of molecular weights). Increasing the number of slices from 100 to 200 gave no appreciable changes. The differential molecular weight distributions of all samples, expressed as $f(M_i) = M_i\phi_i$, are shown in Figures 1 and 2.

Dielectric Measurements. Dielectric loss spectra were obtained for all samples in a parallel-plate geometry, as schematically illustrated in Figure 3; a Hewlett Packard 4284A impedance analyzer was used as described in an earlier paper.[29] The circular electrode had each an area of 29.2 cm², yielding a capacitance of 32.5 pF with air as the dielectric. One electrode was equipped with a guard ring to reduce fringe effects. The plates were separated by a 760-μm Teflon spacer placed in the outer guard-ring region. Polymer was loaded between the electrodes by squeezing, and care was taken to ensure that no bubbles were entrained. A hollow external metal jacket confining the electrodes served as both an electrical shield and as a heating/cooling element. Thermostatic conditions were achieved by flowing through the jacket an ethylene glycol/water mixture, fed from a thermostatic recirculator. All electrical connections were shielded, and leads were kept as short as possible to minimize stray impedances. Thermocouples were mounted on the bottom and top plates; at 373 K the thermocouple readings differed by at most 3 K. Dielectric measurements were performed at several temperatures ranging between 257 and 373 K, at frequencies

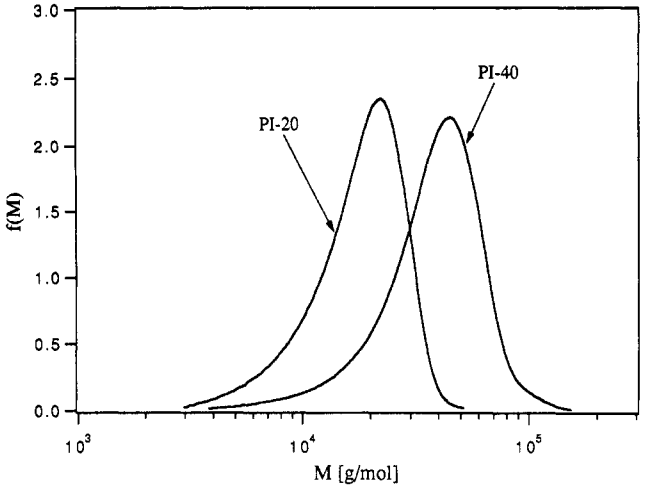

Figure 2. Differential molecular weight distributions of PI-20 and PI-40, expressed as $f(M_i) = M_i\phi_i$.

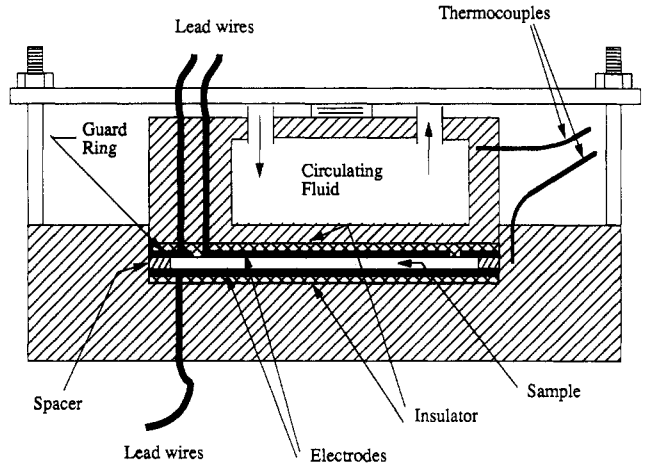

Figure 3. Schematic of parallel-plate apparatus used for dielectric measurements. The circular electrodes have an area of 29.2 cm^2 and are separated by a 760-μm Teflon spacer. One electrode is equipped with a guard ring to reduce fringe effects. The hollow external metal jacket serves as both an electrical shield and a heating/cooling element.

spanning from 100 Hz to 1 MHz, with a 500-mV (peak-to-peak) testing voltage. The temperature was often cycled and measurements were repeated at selected temperatures; reproducibility was good (within 5% or better).

cis-Polyisoprene obeys time–temperature superposition.[19-27,29] The loss spectra were referenced to a temperature of 303 K through the use of an experimental shift factor. The shifts are plotted in Figure 4 along with fits using a Vogel–Fulcher–Tamman (VFT) correlation as described previously[29] and a Williams–Landel–Ferry (WLF) equation with parameters determined by Boese and Kremer.[22] The WLF equation gives a slightly better fit over the VFT correlation.

As shown in eq 15 the magnitude of the dielectric loss should scale as the ratio of density over absolute temperature.[24] When normalized by the ratio ρ/T, the loss spectra still showed a vertical mismatch of about ±5%. Thermal variations in the thickness of the Teflon spacer were the most likely source for this discrepancy. Therefore, the dielectric loss master-curves were constructed by matching vertically the overlapping portions of the shifted spectra. The shapes of the spectra obtained in this manner were highly reproducible. To facilitate comparison with theoretical predictions, all experimental curves were renormalized by the peak value of a reference spectrum, chosen to be that of Lir30.

Results and Discussion

Five combinations of mixing rules and relaxation functions were considered: (i) Tsenoglou mixing rule (eq 7) with the des Cloizeaux TDD (eqs 8–12), (ii) DE mixing (eq 6) with TDD, and (iii) DE mixing with the square root of eq 8 (i.e., using $\varphi(t,\tau_i)$ instead of $\psi(t,\tau_i)$), (iv) Tsenoglou mixing with DER relaxation (eqs 2 and 4), (v) DE mixing with DER relaxation (eqs 2 and 4, with $n = 3.70$). The predicted loss curves were referenced to the peak loss of the predicted Lir30 spectrum. For calculations involving the DER relaxation function, parameters τ_0 and M_0 in eq 4 were obtained by matching the peak frequencies of the predicted Lir30 spectra with the Lir30 data. For the TDD model, M^* and τ^* were chosen according to either of the following two criteria: (1) correct prediction of the experimental peak frequencies of all spectra or (2) correct matching of both the shape and peak position of the Lir30 spectrum. (The relation $M^* = 12.5M_e$ (with $M_e = 5.5$ kg/mol) used by Wasserman and Graessley[11] gave very poor predictions for both the molecular weight dependence of relaxation times and the shapes of the loss spectra. Therefore, M^* was treated as an adjustable parameter.) Calculated model parameters are given in Table II.

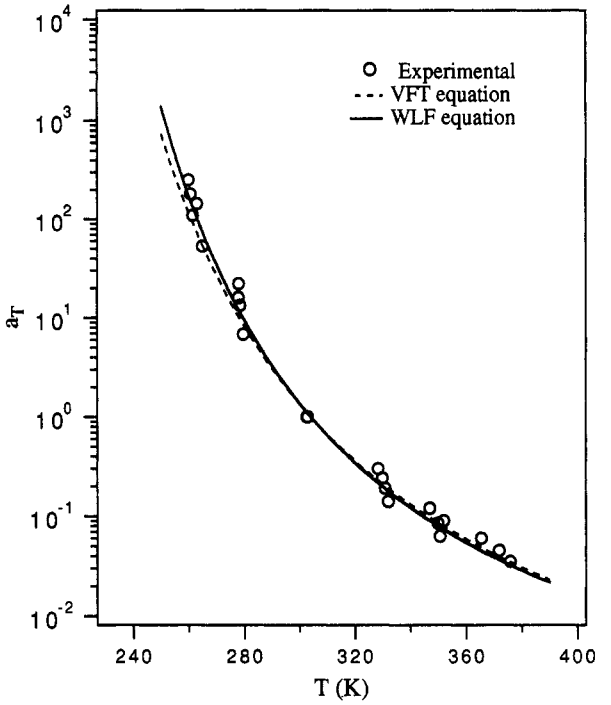

Figure 4. Experimental shift factors, a_T, plotted along with fits using a Vogel–Fulcher–Tamman (VFT) correlation as described in ref 29 and a Williams–Landel–Ferry (WLF) equation, with parameters given by Boese and Kremer.[22]

Table II. Model Parameters for the Various Combinations of Mixing Rules and Relaxation Functions (Reference Temperature = 303 K)

mixing rule/relaxation function	case	criteria[a]	τ^* (Hz^{-1})	M^* [b]
Tsenoglou/TDD	i	1	3.00×10^{-4}	5.00
		2	1.52×10^{-7}	0.50
DE/TDD	ii	1	3.10×10^{-3}	10.0
		2	6.50×10^{-9}	0.20
DE/modified TDD	iii	1	2.70×10^{-4}	8.00
		2	2.72×10^{-6}	2.00

mixing rule/relaxation function	case	τ_0 (Hz^{-1})	M_0[b]
Tsenoglou/DER	iv	7.50×10^{-3}	23.5
DE/DER	v	4.45×10^{-3}	23.5

[a] Criteria: (1) correct prediction of the experimental peak frequencies of all spectra; (2) correct matching of both the shape and peak position of the Lir30 spectrum. [b] In kg/mol.

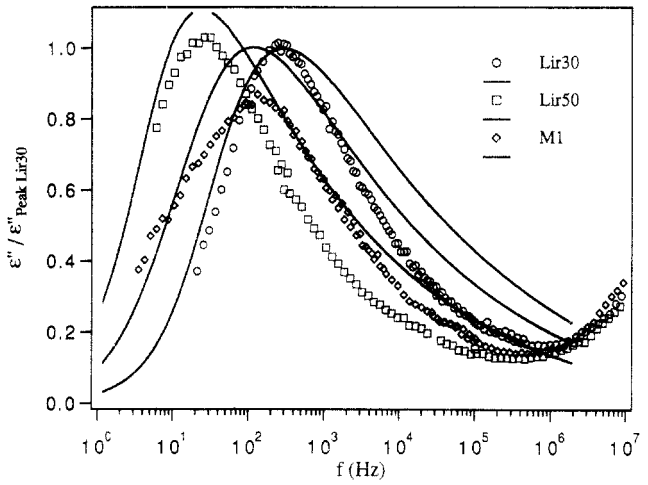

Figure 5. Comparison between predictions based on the Tsenoglou mixing rule and TDD (referred to as case i in the text) with Lir30, Lir50, and M1 data. Parameters M^* and τ^* were chosen to give the correct peak-frequency dependence on molecular weight.

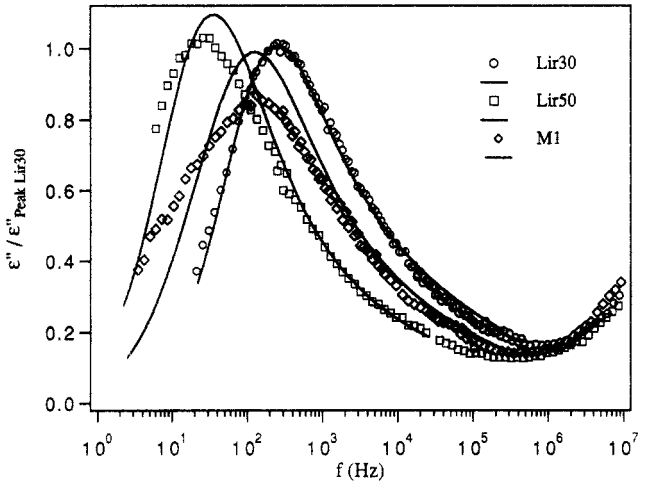

Figure 6. Comparison between predictions based on the Tsenoglou mixing rule and TDD (referred to as case i in the text) with Lir30, Lir50, and M1 data. Parameters M^* and τ^* were chosen to correctly match the shape and position of the Lir30 spectrum.

Predictions based on the Tsenoglou mixing rule and TDD are compared in Figure 5 to the Lir30, Lir50, and M1 data. Here, parameters M^* and τ^* were chosen to give the correct peak-frequency dependence on molecular weight. The calculations capture neither the magnitude nor the broadness of the experimental curves (recall that the peak loss of the Lir30 data was used as a reference). Figure 6 shows predictions when M^* and τ^* are chosen to correctly match the shape and position of the Lir30 spectrum. It can be seen that the Lir30 data are fitted quite well but that discrepancies are still appreciable in the other spectra.

We also considered combination of the DE mixing with two versions of the TDD model: case ii using eq 8 and case iii by replacing $\psi(t)$ with $\varphi(t)$ in eq 9. These combinations were attempted on purely empirical grounds. The outermost exponent of 2 in eq 8 reflects binary interactions[16] and is, in fact, inconsistent with linear mixing. Case iii is a simple-minded attempt to overcome this incongruence by eliminating the square. (Note, however, that $\varphi(t)$ in eq 9 does not approach the DER limit for $H \to \infty$. The cosine transforms (eq 14) of the DER function and eq 8 approach both a $\omega^{-1/2}$ dependence at high frequencies, regardless of H (eq 11). The transform of $\varphi(t)$ scales as $\omega^{-1/4}$ at high frequencies.)

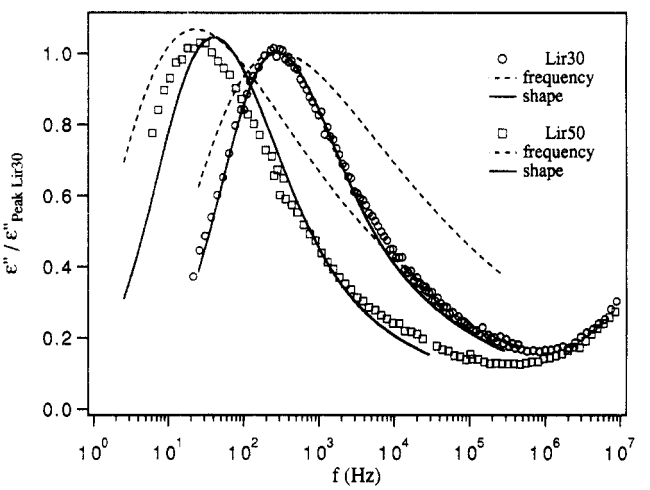

Figure 7. Comparison between predictions based on the DE mixing rule and TDD (referred to as case ii in the text) with Lir30 and Lir50 data. Parameters M^* and τ^* were chosen to (1) give the correct peak-frequency dependence on molecular weight (dashed lines) and (2) match the shape and position of the Lir30 spectrum (solid lines).

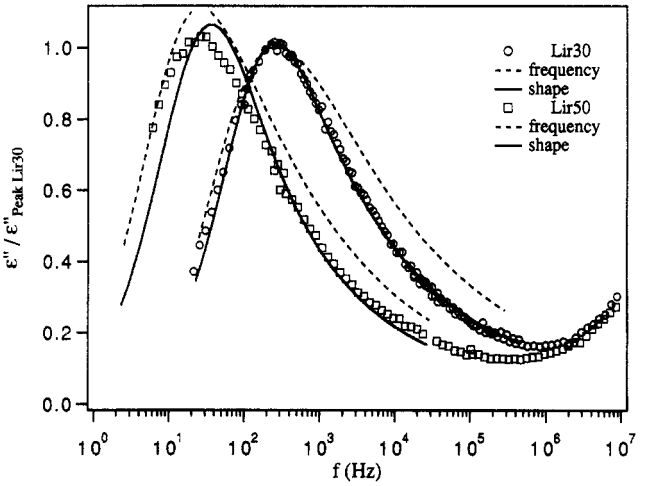

Figure 8. Comparison between predictions based on the DE mixing rule and modified TDD (referred to as case iii in the text) with Lir30 and Lir50 data. Parameters M^* and τ^* were chosen to (1) give the correct peak-frequency dependence on molecular weight (dashed lines) and (2) match the shape and position of the Lir30 spectrum (solid lines).

Figures 7 and 8 compare predictions for cases ii and iii, respectively, with the Lir30 and Lir50 data. Both figures show calculations for the cases in which either the peak positions (dashed lines) or the Lir30 spectrum (continuous lines) were matched (the corresponding values of M^* and τ^* are given in Table II). Although case iii seems to offer a slight improvement over case ii, the overall performance is still quite unsatisfactory.

Predictions based on the Tsenoglou mixing rule and DER relaxation are shown in Figure 9. Here the comparison between the experimental data and the predictions is satisfactory for Lir30 and lir50, but the predicted M1 spectrum is much narrower than the experimental one.

Predictions based on the DE mixing rule and DER relaxation function are shown in Figure 10. In this case the agreement is very good for all the curves. Note again that the curves in Figure 10 have been predicted (including that of Lir30) from the sole knowledge of (1) the molecular weight distribution as measured by SEC, (2) the measured 3.70 power law exponent in eq 4 (this exponent can also be measured rheologically[26]), (3) the magnitude and frequency position of the loss peak of Lir30 (the latter

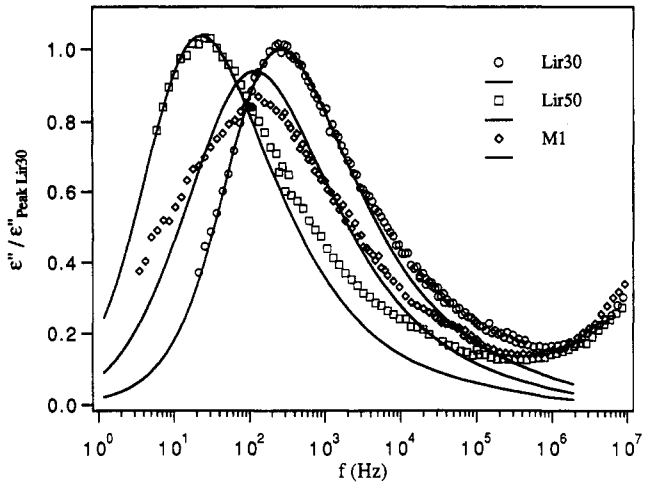

Figure 9. Comparison between predictions based on the Tsenoglou mixing rule and DER relaxation (referred to as case iv in the text) with Lir30, Lir50, and M1 data.

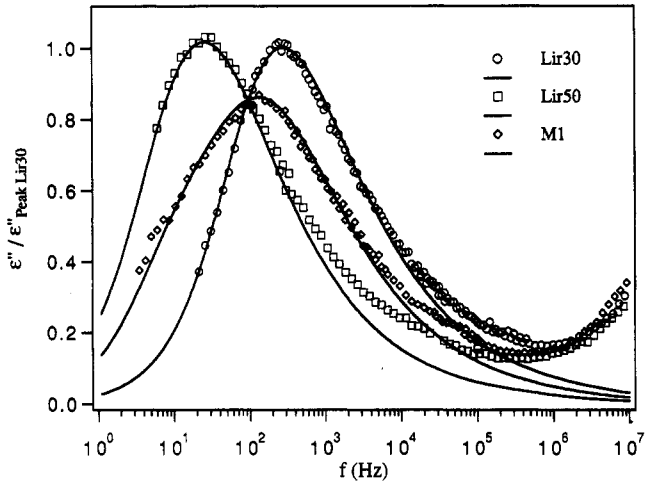

Figure 10. Comparison between predictions based on the DE mixing rule and DER relaxation (referred to as case v in the text) with Lir30, Lir50, and M1 data.

fixes parameters M_0 and τ_0 in eq 4). Aside from these independently measurable quantities no adjustable parameters were used!

Although rather improbable, it is of course always possible that a wrong mixing rule, relaxation function, and power law dependence may have conspired to an overall positive outcome in Figure 10. Fortunately, from the available data it is possible to independently test the validity of the mixing rule alone. Recall that sample M1 was obtained by blending together Lir30 and Lir50 in approximately equal proportions by weight. In Figure 11 the loss data for M1 have been plotted along with a linear combination of the experimental Lir30 and Lir50 spectra:

$$\epsilon''_{mix} = \alpha\epsilon''_{Lir30} + (1-\alpha)\epsilon''_{Lir50} \qquad (18)$$

where ϵ''_{mix} is the linear combination, α is the known mass fraction of Lir30 ($\alpha = 0.519$), and ϵ''_{Lir30} and ϵ''_{Lir50} are the experimental spectra. The linear combination captures very well the behavior of the mixture in the normal-mode region, indicating that linear mixing is indeed valid. Equation 18 contains no assumptions about either chain dynamics models or the dependence of relaxation time on molecular weight. Therefore, the above agreement combined with the results in Figure 10 constitute strong indirect proof of the validity of the DER relaxation function and eq 4, with $n = 3.70$.

The validity of linear mixing implies that, for our system, the species' relaxation times were insensitive to composition. This is in contrast with the results of Adachi et al.[25,27] mentioned earlier in the Introduction. Accordingly, the reader is cautioned that the present results may be limited to systems where the molecular weight distribution is not extremely broad.

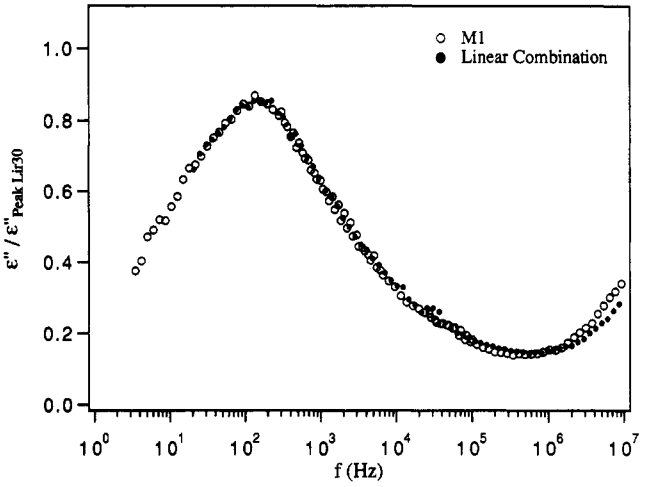

Figure 11. Experimental loss spectrum for M1 (open symbols) plotted along with a linear combination of the experimental Lir30 and Lir50 spectra (eq 18 in the text) (filled symbols).

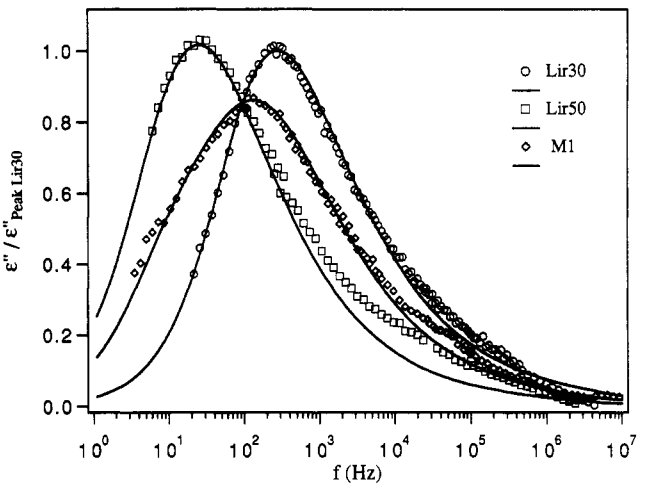

Figure 12. Comparison between predictions based on the DE mixing rule and DER relaxation with Lir30, Lir50, and M1 data corrected for segmental relaxation.

The deviation between data and predictions in Figure 10 at high frequencies could be attributed to two effects: (1) the segmental- and the normal-mode peaks begin to overlap; (2) for low molar mass chains, approaching the entanglement threshold, the power law exponent of the relaxation time may change from 3.7 to 2.0, reflecting the transition to a Rouse behavior.

The segmental peak is insensitive to polydispersity or molecular weight and can be subtracted from the spectra. Havriliak–Negami[32,33] parameters for segmental relaxation have been given by Boese and Kremer.[22] Before subtraction, the calculated segmental spectrum was renormalized to 303 K using the shift factors in Figure 4. In Figure 12 we have replotted the predictions of Figure 10 along with the Lir30, Lir50, and M1 data corrected for segmental relaxation. Similar plots for the samples prepared in our laboratory are shown in Figure 13. At high frequencies the normal mode spectra are still underpredicted. This discrepancy increases with increasing molecular weight, suggesting that it may be linked to a Rouse stretching mode within the entangled regime, as proposed by Adachi and Kotaka.[20] Note that the dis-

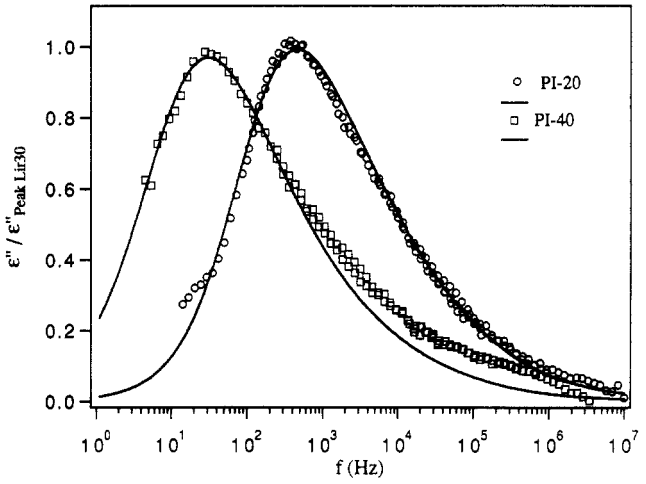

Figure 13. Comparison between predictions based on the DE mixing rule and DER relaxation with PI-20 and PI-40 data corrected for segmental relaxation.

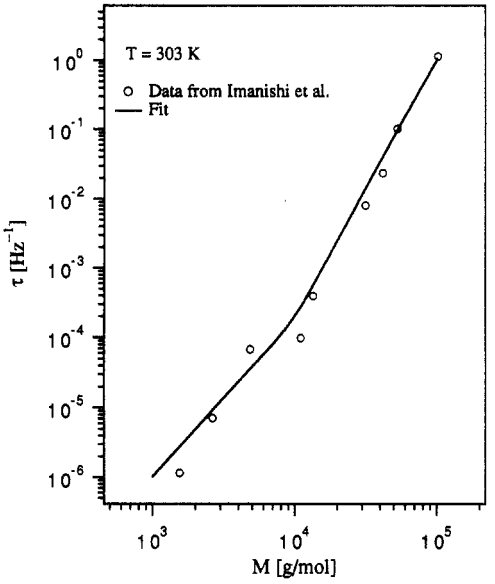

Figure 14. Dielectric normal-mode relaxation times versus molecular weight data of Imanishi et al.[24] shifted to 303 K along with the fit given by eq 19 and 20.

crepancy is much less severe than that expected on the basis of a comparison with a presumed monodisperse system. Furthermore, the agreement seems to improve at lower molecular weights (see sample PI-20 in Figure 13).

All samples used in this study contained small amounts of unentangled or low molecular weight chains for which the relaxation times would be expected to follow an M^2 dependence rather than the 3.7 power law.[24] In Figure 14 we have plotted on a log–log scale the relaxation times versus molecular weight data of Imanishi and co-workers[24] shifted to 303 K. Superposed to the data is a fit of the form

$$\tau = \beta(M/M_c)^n \tag{19}$$

where

$$n = 3.7 - \frac{(3.7 - 2.0)}{(1 + (M/M_c)^4)} \tag{20}$$

with $\beta = 2.0 \times 10^{-4}$ (Hz^{-1}) and $M_c = 10$. Equations 19 and 20 ensure a smooth transition between the high and low molecular weight power law asymptotes.

In an attempt to improve the agreement at high frequencies, calculations with the DE mixing rule and DER relaxation function were repeated using eqs 19 and 20 to replace eq 4. Only the predictions for PI-20 (the sample with the lowest molecular weight) showed noticeable changes and, unfortunately, in the wrong direction, as can be seen in Figure 15. Therefore, this mechanism cannot account for the high-frequency discrepancy. (Note that the data in Figure 14 embody the effect of "self-plasticization" with decreasing molecular weight, as they were not normalized to the isofriction state, as suggested in refs 24–27. Consequently, the change of slope below 10 kg/mol is ill-pronounced and the 3.7 power law extrapolated to molecular weights well below M_c (say, to 2 kg/mol) still affords a reasonable description of the data (within the noise). Such compensation may account for the observed insensitivity of the dielectric loss to the transition. Additionally, Adachi et al.[25,27] have remarked that $M_e = M_c/2$ could indeed be lower than 5 kg/mol; this would further contribute to the smoothing.)

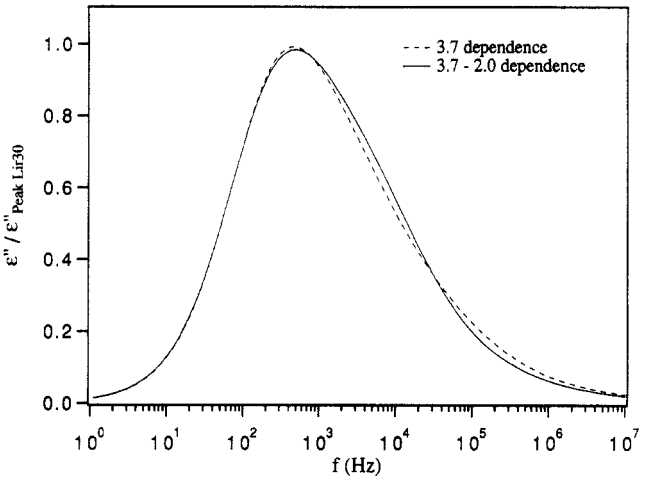

Figure 15. Comparison between predictions based on the DE mixing rule and DER relaxation using a 3.7 power law dependence of relaxation time on molecular weight (dashed line) and using the relaxation time dependence given by eqs 19 and 20 (solid line).

Granted the success of the Doi–Edwards model, it is now possible to obtain feedback regarding the effect of small degrees of polydispersity on the normal-mode dielectric loss. This point was raised in the Introduction with regard to the work of Imanishi et al.[24] Molecular weight distributions of anionically-synthesized polymers can often be approximated as a Schultz distribution:[34]

$$\phi_i = \frac{a}{x_n\Gamma(a+1)}\left(\frac{ax_i}{x_n}\right)^a \exp\left(-\frac{ax_i}{x_n}\right) \tag{21}$$

where ϕ_i is the weight fraction of the species with degree of polymerization x_i, x_n is the number average degree of polymerization, $\Gamma(X)$ is the gamma function, and a is related to the breadth of the distribution ($M_w/M_n = x_w/x_n = (a+1)/a$).

Figure 16 shows predicted loss spectra for three different distributions: (1) monodisperse distribution, (2) Schultz distribution with $M_w/M_n = 1.04$ ($a = 25$), and (3) an experimental distribution obtained from SEC of a *cis*-PI standard with $M_w/M_n = 1.04$ (the standard was purchased from Polymer Laboratories Inc.). The spectra have all been renormalized by their peaks. Two features are noteworthy: (1) the prediction using a Schultz distribution matches fairly well that from the experimental distribution; (2) significant deviations from the monodisperse case are still noticeable down to $M_w/M_n = 1.04$ (samples in this limit are often considered monodisperse). The half-widths of the $M_w/M_n = 1.04$ spectrum in Figure 16 are in good

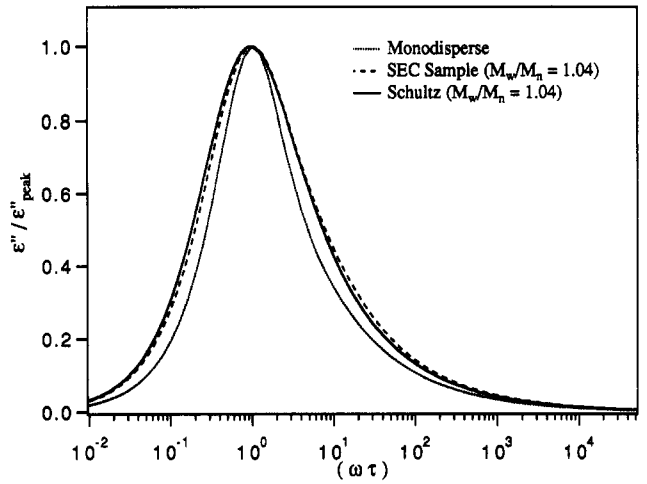

Figure 16. Predicted loss spectra for three different distributions: (1) monodisperse (dotted line), (2) Schultz distribution with M_w/M_n = 1.04 (solid line), and (3) an experimental distribution obtained from SEC of a *cis*-PI standard with M_w/M_n = 1.04 (dashed line).

agreement with the data of Imanishi et al.[24] This implies that, in approaching the reptation limit the high-frequency half-width undergoes a swift drop below M_w/M_n = 1.04, so that linear extrapolation from above 1.04 is improper. This explains the discrepancy in the limiting half-widths reported by Imanishi and co-workers.[24] This point will be examined in greater detail in an upcoming publication.

Conclusion

We have considered the prediction of the dielectric normal-mode process in polydisperse melts of *cis*-polyisoprene above entanglement. Predictions by several combinations of mixing rules and autocorrelation functions were examined and compared to experimental data.

Within the range of molecular weights considered, quantitative predictions were obtained only with the Doi–Edwards mixing rule and the relaxation function of classical reptation (DER). Different from classical reptation, however, a 3.70 power law exponent of the relaxation time on molecular weight was required to match simultaneously the peak frequencies and the broadness of the spectra.

Linear mixing holds regardless of the assumed chain relaxation model, thereby confirming indirectly the validity of the reptation model. This indicates that, in our range of molecular weights and polydispersities, the species' relaxation times are insensitive to matrix composition. Caution should be exerted, however, in extrapolating the present results to systems with extremely broad MWD or to polymers with stronger dipolar interactions.

Compared to rheological predictions[11] (which seem to require the use of more complex mixing rules), the present results seem to indicate different sensitivities of dielectric and viscoelastic relaxation to entanglement effects. This sensitivity may be useful in devising tests for the entanglement and reptation hypotheses.

Rudimentary attempts to account for a transition from $M^{3.7}$ to M^2 of the relaxation time did not improve but, in fact, slightly degraded the predictions at high frequencies. Even after accounting for segmental relaxation, the high-frequency mismatch between theory and experiments increased with molecular weight. Rouse relaxation acting in parallel with reptation could be a source for this discrepancy. Polydispersity effects were shown to be important even down to M_w/M_n = 1.04; a more detailed study of these effects will appear shortly. Inversion of dielectric loss spectra to obtain the polymer molecular weight distribution is now a justifiable endeavor, to be considered in an upcoming publication.

Acknowledgment. We gratefully acknowledge the donors of the Petroleum Research Fund, administered by the American Chemical Society (Grant ACS-PRF24927-G7B) and the National Science Foundation (Grant CTS-9208478) for partial support of this research. We also thank two anonymous reviewers for their constructive criticism.

Appendix A

We seek an asymptotic expansion as $x \to 0$ for the following function:

$$f(x) = \sum_{\substack{p=1 \\ p\ \text{odd}}}^{\infty} \frac{1}{p^2} \exp(-p^2 x) \tag{A1}$$

Knowing that $f(0) = \pi^2/8$, we convert the summation over p into a summation over n and rearrange the equation as follows

$$f(x) = \frac{\pi^2}{8} - \sum_{n=0}^{\infty} \frac{(1 - \exp(-(2n+1)^2 x))}{(2n+1)^2} \tag{A2}$$

For $x \ll 1$ the summation can be converted into a Riemann integral[35]

$$f(x) \approx \frac{\pi^2}{8} - x^{1/2} \int_0^{\infty} \frac{(1 - \exp(-4t^2))}{4t^2}\, dt \tag{A3}$$

therefore, to leading order

$$f(x) \approx \frac{\pi^2}{8} - (\pi x)^{1/2} \quad \text{for} \quad x \le 0.10 \tag{A4}$$

Equation A4 was checked against exact calculations using 5×10^5 terms in eq A1; for $x \le 0.20$ the approximation is accurate to within 10^{-4}%. For $x \ge 0.20$ only 12 terms are necessary in eq A1 to converge to the virtually exact result.

Similar to the above results we can also find an approximation for

$$g(x) = \sum_{n=0}^{\infty} \frac{(1 - \exp(-n^2 x))}{n^2} \tag{A5}$$

as $x \to 0$. In this case we demand a little more accuracy than for $f(x)$, since $g(x)$ appears in an exponential (eqs 9 and 10 in the text). We obtain

$$g(x) \approx (\pi x)^{1/2} - \frac{x}{2} \quad \text{for} \quad x \le 0.50 \tag{A6}$$

This approximation is sound to within 10^{-4}% for $x \le 0.50$ (this result was checked with a vectorized algorithm using 10^6 terms in the summation). For $x \ge 0.50$ eq A5 converges within only 10 terms.

Appendix B

Consider function $f(x)$ absolutely integrable over the domain $(0 \le x < \infty)$ and such that $f(0) = 1$. We wish to

calculate the following one-sided transform

$$F(\omega) = \int_0^\infty f(z/\omega)\cos(z)\,dz \tag{B1}$$

in the limit $\omega \to \infty$. We first subdivide the integral as follows:

$$F(\omega) = \int_0^{\pi/2} f(z/\omega)\cos(z)\,dz + \sum_{n=0}^{\infty}\int_{\pi/2+2\pi n}^{\pi/2+2\pi(n+1)} f(z/\omega)\cos(z)\,dz \tag{B2}$$

As $\omega \to \infty$, $f(z/\omega)$ is stretched out along the z axis and the following approximation can be adopted in each subinterval:

$$f(x) \cong f(x_n) + \frac{[f(x_{n+1}) - f(x_n)]}{[x_{n+1} - x_n]}(x - x_n) + O[(x - x_n)^2] \tag{B3}$$

so that

$$\int_{\pi/2+2\pi n}^{\pi/2+2\pi(n+1)} f(z/\omega)\cos(z)\,dz \cong \int_{\pi/2+2\pi n}^{\pi/2+2\pi(n+1)}\left(f(x_n) + \frac{[f(x_{n+1}) - f(x_n)]}{[x_{n+1} - x_n]}(x - x_n)\right)\cos(z)\,dz \tag{B4}$$

where $x \equiv z/\omega$. Straightforward integration and rearrangement give

$$\int_{\pi/2+2\pi n}^{\pi/2+2\pi(n+1)} \frac{[f(x_{n+1}) - f(x_n)]}{[x_{n+1} - x_n]}(x - x_n)\cos(z)\,dz = \frac{[f(x_{n+1}) - f(x_n)]}{[x_{n+1} - x_n]}\frac{2\pi}{\omega} = f(x_{n+1}) - f(x_n) \tag{B5}$$

Therefore,

$$F(\omega) \cong \int_0^{\pi/2} f(z/\omega)\cos(z)\,dz + \sum_{n=0}^{\infty} f(x_{n+1}) - f(x_n) \quad \text{for} \quad \omega \to \infty \tag{B6}$$

Alternating terms in the summation cancel each other, giving

$$F(\omega) \cong \int_0^{\pi/2} f(z/\omega)\cos(z)\,dz - f(\pi/2\omega) \quad \text{for} \quad \omega \to \infty \tag{B7}$$

More generally, one may also write

$$F(\omega\to\infty) \cong \int_0^{\pi/2+2\pi\nu} f(z/\omega)\cos(z)\,dz - f((\pi/2+2\pi\nu)\omega) \quad \text{for} \quad \nu \geq 0,\ \nu \in N \tag{B8}$$

which enables one to achieve greater precision if required.

The autocorrelation function meets the above criteria and eq B8 can be used to calculate ϵ''. For the numerical calculations we used the following relation:

$$F(\omega) = \int_0^{\pi/2} f(z/\omega)\cos(z)\,dz + \sum_{n=0}^{n^*}\int_{\pi/2+2\pi n}^{\pi/2+(n+1)2\pi} f(z/\omega)\cos(z)\,dz - f(\pi/2+2n^*\pi) \tag{B9}$$

where n^* pinpoints the term at which the approximation becomes valid. The value of n^* was chosen to verify that (1) the numerically performed integral (by quadrature) from $(n^* - 1)$ to n^* was with 0.01% of the value given by the approximation (eq B5) and (2) the slope of function $f(x)$ changed by no more than 0.01% across the integration interval.

References and Notes

(1) Dealy, J. M.; Wissbrun, K. F. *Melt Rheology and Its Role in Plastics Processing*; van Nostrand Reinhold: New York, 1989.
(2) Kurata, M. *Macromolecules* **1984**, *17*, 895.
(3) Struglinski, M. J.; Graessley, W. W. *Macromolecules* **1985**, *18*, 2630.
(4) Rubinstein, M.; Colby, R. H. *J. Chem. Phys.* **1988**, *89* (8), 5291.
(5) Münstedt, H. *J. Rheol.* **1980**, *24*, 847.
(6) Doi, M.; Edwards, S. F. *The Theory of Polymer Dynamics*; Oxford University Press: New York, 1989.
(7) de Gennes, P. G. *J. Chem. Phys.* **1971**, *55*, 572.
(8) Doi, M.; Edwards, S. F. *J. Chem. Soc., Faraday Trans. 2* **1978**, *74*, (Parts 1-3), 1789.
(9) Rouse, P. E. *J. Chem. Phys.* **1953**, *21* (7), 1272.
(10) Zimm, B. H. *J. Chem. Phys.* **1956**, *24* (2), 269.
(11) Wasserman, S. H.; Graessley, W. W. *J. Rheol.* **1992**, *36* (2), 543.
(12) Monfort, J. P.; Marin, G.; Monge, P. *Macromolecules* **1984**, *17*, 1551.
(13) Graessley, W. W. *Adv. Polym. Sci.* **1982**, *47*, 68.
(14) Doi, M.; Graessley, W. W.; Helfand, E.; Pearson, D. S. *Macromolecules* **1987**, *20*, 1900.
(15) Marrucci, G. *J. Polym. Sci., Polym. Phys. Ed.* **1985**, *23*, 159.
(16) des Cloizeaux, J. *Macromolecules* **1990**, *23*, 4678, 3992; **1992**, *25*, 835.
(17) Tsenoglou, C. *Macromolecules* **1991**, *24*, 1762.
(18) Stockmayer, W. H. *Pure Appl. Chem.* **1967**, *15* (3), 247.
(19) Adachi, K.; Kotaka, T. *Macromolecules* **1984**, *17*, 120.
(20) Adachi, K.; Kotaka, T. *Macromolecules* **1985**, *18*, 466.
(21) Riande, E.; Saiz, E. *Dipole Moments and Birefringence of Polymers*; Prentice Hall: Englewood Cliffs, NJ, 1992.
(22) Boese, D.; Kremer, F. *Macromolecules* **1990**, *23*, 829.
(23) Adachi, K.; Kotaka, T. *Macromolecules* **1988**, *21*, 157.
(24) Imanishi, Y.; Adachi, K.; Kotaka, T. *J. Chem. Phys.* **1988**, *89* (12), 7585.
(25) Adachi, K.; Itoh, S.; Nishi, I.; Kotaka, T. *Macromolecules* **1990**, *23*, 2550.
(26) Adachi, K.; Yoshida, H.; Fukui, F.; Kotaka, T. *Macromolecules* **1990**, *23*, 3138.
(27) Adachi, K.; Itoh, S.; Nishi, I.; Kotaka, T. *Macromolecules* **1990**, *23*, 2554.
(28) Graessley, W. W. *Faraday Symp. Chem. Soc.* **1983**, *18*, 7.
(29) Fodor, J.; Hill, D. A. *Macromolecules* **1992**, *25*, 3511.
(30) Morton, M.; Fetters, L. J. *Anionic Polymerization: Principles and Practices*; Academic Press: New York, 1983.
(31) Tanaka, Y.; Takeuchi, Y.; Kobayashi, M.; Tadokoro, H. *J. Polym. Sci., Polym. Phys. Ed.* **1971**, *9*, 43.
(32) Havriliak, S.; Negami, S. *J. Polym. Sci., Part C* **1966**, *14*, 99.
(33) Havriliak, S.; Negami, S. *Polymer* **1967**, *8*, 161.
(34) Rodriguez, F. *Principles of Polymer Science*, 3rd ed.; Hemisphere Publishing Corp.: New York, 1989.
(35) Bender, C. M.; Orszag, S. A. *Advanced Mathematical Methods for Scientists and Engineers*; McGraw-Hill: New York, 1978.